A passive permanent magnetic bearing with increased axial lift relative to radial stiffness

Nielsen, Kaspar Kirstein; Bahl, Christian; Dagnæs-Hansen, Nikolaj Aleksander; Santos, Ilmar ; Bjørk, Rasmus

Published in:
IEEE Transactions on Magnetics

Link to article, DOI:
10.1109/TMAG.2020.3042957

Publication date:
2021

Document Version
Peer reviewed version

A passive permanent magnetic bearing with increased axial lift relative to radial stiffness

K. K. Nielsen[1], C. R. H. Bahl[1], Nikolaj A. Dagnaes[2], Ilmar F. Santos[2], R. Bjørk[1]

[1]Department of Energy Conversion and Storage, Technical University of Denmark - DTU, Anker Engelunds Vej, Building 301, 2800 Kgs. Lyngby, Denmark
[2]Department of Mechanical Engineering, Technical University of Denmark - DTU, Nils Koppels Alle, Building 404, 2800 Kgs. Lyngby, Denmark,
e-mail: rabj@dtu.dk

***Abstract*—Four different magnet bearing configurations, with varying numbers of combined radially and axially magnetized rings, are studied both experimentally and using the modeling framework MagTense. First the optimal vertical position of the radially magnetized ring is determined using the numerical model. Then the model is validated using experimental data. Finally, we show that a bearing where the rotor and the stator each consist of a single ring of axially magnetized magnets and a single ring of radially magnetized magnets has the smallest radial force per axial lift force at an axial air gap of 1 mm. For this bearing, the ratio of the radial force per axial lift here is 0.383 times that of the same bearing without the radially magnetized ring.**

I. Introduction

Stable passive magnetic levitation of non-diamagnetic materials is not possible as proven by the British mathematician Samuel Earnshaw in 1842 [1]. However, if a force is introduced that constantly corrects the position of the levitated object, levitation may be achieved. Such a force is typically called an active force, as it cannot be provided by a constant magnetic field. Levitation is also possible as a result of a gyroscopic effect [2, 3]. Here we consider the former case, i.e. where an active force component is used to keep an object centered in order to compensate the negative radial stiffness. In such a system, the lifting needed for levitation of the object in question is provided by a passive magnetic bearing and the continuous position correction is done by an active magnetic bearing. The less negative the radial stiffness of the passive bearing is, the less force and thus energy is required by the active bearing to keep the object in equilibrium. These types of magnetically levitated bearings can be constructed with energy losses orders of magnitude below the friction of comparable mechanical bearings.

One of the simplest configurations of a passive bearing is to have two axially magnetized concentric rings at different axial positions. Such a system was theoretically studied by Yonnet [4], who found that the lifting strength and stiffness were the same if the rings were magnetized radially instead. Since then, the interaction energy between the magnets in the different parts of the bearing has been used to calculate the stiffness for bearings in 2D [5]. For a system of two ring permanent magnets with axial magnetization the levitation force has been found in closed-form expression [6] and the stiffness has been found semi analytically [7] and similarly for a system with radial magnetization [8], and for bearings with alternate magnetization directions corresponding to Halbach structures [9]. This latter configuration was shown to provide a high axial stiffness. Fully analytical expressions for stiffness and peak load in radial magnetic bearings have also been found [10] and used to provide rules-of-thumb of the axial load for designs using NdFeB magnets. A combination of a radially magnetized bottom ring and an axially magnetized smaller top ring has also been studied, with the axial force of this configuration determined for various sizes using a semi analytical approach [11]. A number of experimental investigations have also been performed, e.g. on radial magnetic bearings with an axial offset. Here magnets with various arc-lengths were investigated, and the conclusion is that the longer the arc length, the higher the load capacity [12]. Finally, the load-carrying capacity and the radial and axial stiffness for an axial magnetized bearing has been investigated both analytically, numerically and experimentally, with good agreement between the model and experiment, except in the case where high permeability materials are present [13].

The common conclusion to these studies is that the lifting force of a bearing design depends on the size and position of the rings, but with no clear design being ideal. Numerically, the repulsive bearing design that provides maximum radial stiffness has been found [14]. This is determined only by the width of the air gap between rotor and stator. Magnetized rings have also been stacked [15], which reduces the radial stiffness, and also extended to Halbach type structures, where the axial force and stiffness have been calculated for a range of configurations [9, 16]. The active magnetic bearing that maintains the equilibrium position of the passive bearing has also been intensively investigated [17, 18, 19, 20].

Besides the obvious need to study new bearing designs the following shortcomings of the literature also motivates this work: Current numerical methods fail to obtain accurate stiffness estimates due to resolution problems. For systems levitated using active magnetic bearings in combinations with passive magnetic bearings, the perturbations are extremely small compared to the dimensions of the passive bearings. Thus an extremely fine mesh is needed to capture the change in force due to the perturbation. This makes current numerical methods too computationally heavy to accurately estimate the stiffness - for more details see [13]. Secondly, analytical expressions are only available for the case where rotor and

stator are coaxially aligned and the case when all materials have relative permeability close to 1. The method presented here can be used to find an accurate stiffness also when the rotor and stator are not placed coaxially. This is often the case in reality because tolerances and small material variations of the active magnetic bearing makes the geometrical center and the magnetic center not aligned. Furthermore, the method presented here will work when the bearing contains materials with relative permeability different from one which is the case for almost all real passive magnetic bearings.

Here we will investigate new geometries for a passive magnetic bearing, with the goal of examining its trade-off between radial stiffness and lifting strength. In order to realize a novel passive permanent magnetic bearing with lower radial stiffness we first consider a range of different bearing geometries. In these geometries a combination of axial and radial rings is employed. The forces are then found through modeling using the state-of-the-art open source magnetostatics modeling framework MagTense [21] in 3D. Following this, a number of bearings are realized, experimentally characterized and compared with the numerical results, and the model is used to predict the performance of the different bearings in identical configurations.

II. Design

A magnetic bearing is characterized by its lift and stiffness, where the latter will contribute to equilibrium instability. Here lift is the amount of force in the vertical direction provided by the bearing. By scaling up the bearing the lift can be increased, but the relative stiffness of the bearing remains the same. This is a consequence of the fact that the magnetic field scales with the geometry of the bearing, but the absolute lift of the bearing increases as the bearing is made larger. The relative stiffness, which is the gradient of the force with respect to the size of the bearing remains constant however. The stiffness of a bearing, $\mathbf{K}$, is the negative of the derivative of the force in a specific direction with respect to the displacement in the same direction, i.e.

$$\begin{aligned}\mathbf{K} &= -\left(\frac{dF_x}{dx}\hat{x}+\frac{dF_y}{dy}\hat{y}+\frac{dF_z}{dz}\hat{z}\right)\\ &= -\left(K_x\hat{x}+K_y\hat{y}+K_z\hat{z}\right).\end{aligned} \tag{1}$$

Here we do not consider the cross couplings stiffnesses, i.e. $\frac{dF_x}{dy}\hat{y}$, as these do not enter in Earnshaws theorem and are thus not needed for calculating the stiffness of the bearing. Earnshaw's theorem says that the sum of the three stiffness components must be zero. For a bearing with radial symmetry $K_x = K_y = K_r$ and thus

$$K_z = -2K_r. \tag{2}$$

The compromise in any bearing is realizing a high value of the lift while maintaining a reasonably low radial stiffness.

We will here consider four different geometries for the passive magnetic bearing. These four different designs are shown as schematics in Fig. 1. The bearing shown in Geometry I is identical to one of the original repulsive passive bearings considered by Yonnet [4], while the design shown in Geometry II has also been considered in Ref. [13]. The two new designs, geometries III and IV, are a combination of axially and radially magnetized concentric rings, whose combination have not previously been studied. In general we denote the part of the bearing with the smallest diameter the rotor, and the one with the largest diameter the stator. What is crucial to note here is that we consider actual bearings that consists of rings of square permanent magnets with a size of $3 \times 3 \times 3$ mm. This means that the bearings are not inherently axisymmetric, as the square magnets have to be placed in the ring round the central axis of the bearing. The dimensions of the bearings are the result of a desired even number of the square permanent magnets in each of the bearing "rings". That number is given in Table I. Each of these four designs was numerically modeled, constructed and tested, as discussed in the following sections. The designs were chosen based on their increasing complexity and include the addition of radially magnetized "rings", which may potentially lower the radial stiffness of the passive bearing.

The bearings were manufactured from aluminium and iron, as previously indicated on the schematic drawing, i.e. Fig. 1. Images of bearings I and IV are shown in Fig. 2. Magnet cubes were carefully fixed in place in the bearing structures using epoxy. The correct orientation of each cube was verified after the curing of the epoxy using a test magnet.

III. Model

In order to numerically evaluate the lift and stiffness of the bearings described above, we utilize the open source magnetostatics modeling framework MagTense [21] to calculate the force between the two parts of the bearings (rotor and stator), as a function of the relative position of these. The bearing is modelled in full 3D. Both variation in the axial distance between the bearing components, termed dz in Fig. 1, as well as displacement of the bearing components in the radial direction, termed dr in Fig. 1, are considered. Again note that actual $3 \times 3 \times 3$ mm magnets placed in rings are considered.

In order to calculate the electromagnetic force on either of the two parts of the bearing the Lorentz force is integrated over a volume entirely covering *one* of the two parts. This can be formulated as two integrals: a surface integral over Maxwell's stress tensor and a volume integral of the Poynting vector [1]:

$$\mathbf{F} = \oint_{S'} \mathbb{T}\cdot \mathrm{d}\mathbf{a} - \epsilon_0\mu_0\frac{\mathrm{d}}{\mathrm{dt}}\int_{V'}\mathbf{S}\mathrm{d}V', \tag{3}$$

with S' denoting the closed surface surrounding one of the two bearing parts having area element $\mathrm{d}\mathbf{a}$, volume V' and volume element $\mathrm{d}V'$, and with ϵ_0 and μ_0 denoting the vacuum permittivity and permeability, respectively. Assuming no electrical fields in the bearing, there will be no time variation of the Poynting vector $\mathbf{S}$ and we are left with Maxwell's stress tensor, where the components are given by

$$T_{ij} = \frac{1}{2}\epsilon_0\left(E_iE_j - \frac{1}{2}\delta_{ij}E^2\right) + \frac{1}{\mu_0}\left(B_iB_j - \frac{1}{2}\delta_{ij}B^2\right). \tag{4}$$

Again, assuming no electric fields, the stress tensor reduces to:

$$T_{ij} = \frac{1}{\mu_0}\left(B_iB_j - \frac{1}{2}\delta_{ij}B^2\right), \tag{5}$$

This article has been accepted for publication in a future issue of this journal, but has not been fully edited. Content may change prior to final publication. Citation information: DOI 10.1109/TMAG.2020.3042957, IEEE Transactions on Magnetics

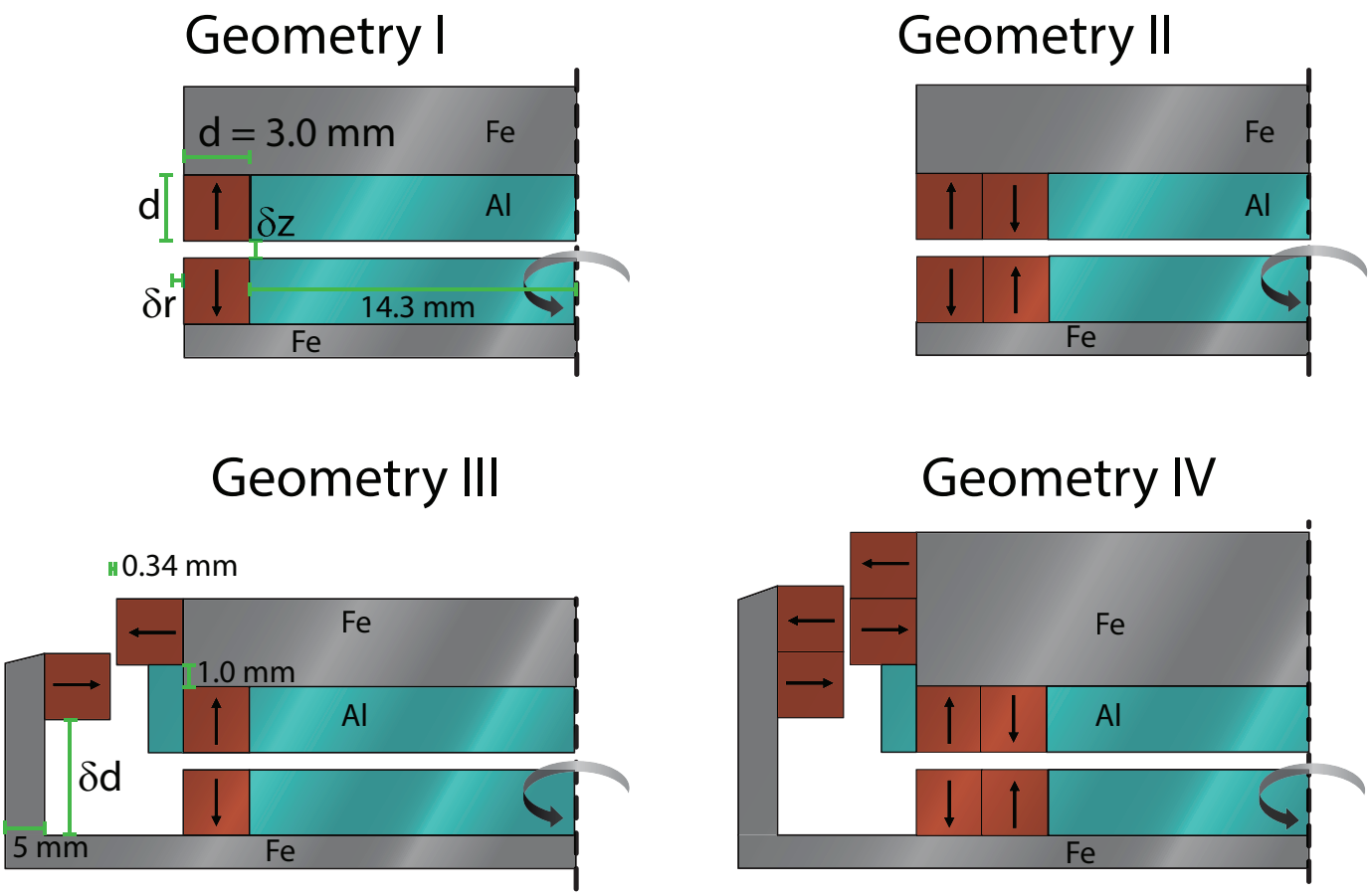

Fig. 1. A schematic illustration of the four different bearing geometries tested. All drawings are axisymmetric, except when a radial displacement δr is introduced, as this breaks the axisymmetry. Note that the actual experimental and modelled bearing have cube magnets and are thus not fully axisymmetric. The direction of magnetization of the individual magnets has been indicated. "Fe" indicates iron parts, which are magnetic, while "Al" indicates non-magnetic aluminium parts.

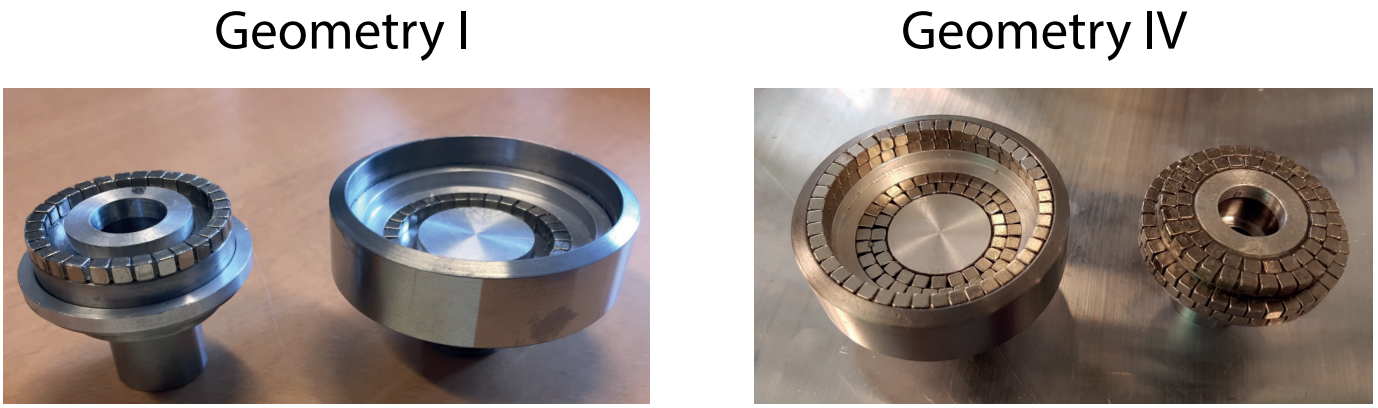

Fig. 2. Images of both parts of bearings I and IV.

where $\mathbf{B} = (B_x, B_y, B_z)$ is the magnetic flux density.

In order to integrate Maxwell's stress tensor over the closed surface S' surrounding one of the two parts of the bearing we thus need the magnetic flux density on this surface. We assume that each of the individual NdFeB cube magnets in the bearings is homogeneously magnetized. However, the relative permeability tensor for these magnets is not exactly unity, so it is necessary to find the magnets' self-consistent magnetization vectors as they interact magnetically both with themselves (through their demagnetizing fields) and each other (through their stray fields).

Assuming a diagonal permeability tensor $\boldsymbol{\mu}_r$ describing the anisotropy of the NdFeB magnets we can write the constitutive relation between the magnetic field $\mathbf{H}$ and the magnetization

TABLE I
PROPERTY SUMMARY OF THE FOUR BEARINGS TESTED. WHEN TWO RINGS ARE PRESENT, THE NUMBER OF MAGNETS IN EACH RING IS GIVEN SEPARATELY.

Bearing	No. of axial magnets	No. of radial magnets	Total no. of magnets
I, rotor	30	0	
I, stator	30	0	60
II, rotor	20 and 30	0	
II stator	20 and 30	0	100
III, rotor	30	37	
III, stator	30	44	141
IV, rotor	24 and 30	37 and 37	
IV, stator	24 and 30	44 and 44	270

$\mathbf{M}$ in such a magnet in the global coordinate system, V:

$$\mathbf{M} = (\boldsymbol{\mu}_r - I)\mathbf{H}^\top + [\mathbf{M}_{\text{rem}}]_V, \tag{6}$$

with the relative permeability in the global coordinate system given by

$$\boldsymbol{\mu}_r = P_i \begin{pmatrix} 1.04 & 0 & 0 \\ 0 & 1.25 & 0 \\ 0 & 0 & 1.25 \end{pmatrix}. \tag{7}$$

The numerical values of the diagonal entries are explained in the experimental section, but it is important to note that the diagonal values are not identical. The change-of-basis matrix from the local coordinate system, V_i', of the i'th cubic magnet to the global coordinate system is denoted P_i. This matrix consists of three unit vectors organized such that the first is along the easy axis of the magnet while the two remaining are along the two mutually perpendicular hard axes

$$P_i = \left\{ [\mathbf{u}_{\text{ea}}^\top]_V; [\mathbf{u}_{\text{ha1}}^\top]_V; [\mathbf{u}_{\text{ha2}}^\top]_V \right\}, \tag{8}$$

all with respect to the global coordinate system, V. The relation above thus transforms the relative permeability from a local coordinate system of the i'th magnet to the global coordinate system. The same applies for the remanence vector of the ith magnet, $[\mathbf{M}_{\text{rem}}]_{V_i'} = \pm M_{\text{rem}}(1,0,0)$ with the sign reflecting the direction of magnetization and M_{rem} denoting the norm of the remanent magnetization set to 1.09 T (see the experimental section). Obtaining the remanence in the global coordinate system is then done via the change-of-basis: $[\mathbf{M}_{\text{rem}}^\top]_V = P_i[\mathbf{M}_{\text{rem}}^\top]_{V_i'}$

In this work the magnets may be either radially or axially magnetized as seen from the global coordinate system. It is therefore necessary to give the transformations for both cases, which is done in the following.

A. Axially magnetized magnets

When the magnets are axially magnetized their easy-axes are always parallel to the z-direction of the global coordinate system. Whether they are magnetized up- or downwards is reflected in the sign of the remanent magnetization. In order to have simple unit vectors along the hard axes we define these to be perpendicular to the relevant faces of the cubic magnets while simultaneously being perpendicular to the easy axis. In this way the actual calculations involving the tensor field formulation discussed below become slightly simpler. The magnets in all configurations in this work will be rotated about the z-axis by an angle θ_i. Thus the change-of-basis matrix P for the ith axially magnetized magnet rotated about the $z-$axis is given by

$$P_{i,\text{axial}}(\theta_i) = \begin{pmatrix} 0 & \cos\theta_i & -\sin\theta_i \\ 0 & \sin\theta_i & \cos\theta_i \\ 1 & 0 & 0 \end{pmatrix}. \tag{9}$$

As this matrix is orthogonal, we have that $P_{i,\text{axial}}^{-1} = P_{i,\text{axial}}^\top$.

B. Radially magnetized magnets

For radially magnetized magnets that are rotated by θ_i about the global $z-$axis one of the hard axis unit vectors is constantly parallel to the $z-$axis while the easy axis unit vector points radially and the remaining hard axis unit vector is simultaneously perpendicular to the two latter unit vectors. Again, following the convention that the first column of the P matrix contains the easy axis, we get for the ith radially magnetized magnet:

$$P_{i,\text{radial}}(\theta_i) = \begin{pmatrix} \cos\theta_i & -\sin\theta_i & 0 \\ \sin\theta_i & \cos\theta_i & 0 \\ 0 & 0 & 1 \end{pmatrix}, \tag{10}$$

and note that this matrix is also orthogonal and so $P_{i,\text{radial}}^{-1} = P_{i,\text{radial}}^\top$. The sign of the remanent magnetization defines whether the magnetization of the radially magnetized magnet points in- or outwards.

C. The tensor field formulation

In order to find the magnetic field, $\mathbf{H}$, at the point $\mathbf{r}$ produced by a homogeneously magnetized cube with cube center at $\mathbf{r}'$ we employ the demagnetization tensor field $\mathbb{N}$:

$$\mathbf{H}(\mathbf{r}) = P\mathbb{N}(P^{-1}(\mathbf{r} - \mathbf{r}')) \cdot P^{-1}\mathbf{M}(\mathbf{r}'), \tag{11}$$

where the index on the P matrix has been omitted for brevity and it is emphasized that the tensor field, $\mathbb{N}$, is found in the local coordinate system of the given magnet. This tensor is known analytically in the case of a homogeneously magnetized rectangular prism [22], and is implemented in the MagTense framework.

In order to find the self-consistent magnetization vectors of each cubic permanent magnet, we apply the superposition principle, find the magnetic field in each magnet produced by itself and all the other magnets using Eq. (11), update the magnetization corresponding to Eq. (6), update the field again and terminate this iteration process once the relative change in

the norm of the magnetization of each magnet is less than 1 ppm. Once the self-consistent magnetization vectors are found we use Eq. (11) to find the field at any desired point $\mathbf{r}$, which in the case of integration of Maxwell's stress tensor (Eq. (5)) lies on the surface integrated over. All of this is done in the MagTense framework [21].

In the model, none of the iron parts included in the schematic is included. The reason for this is that including the very high permeability iron makes the model excessively difficult to converge. However, as the iron parts are only located on the "back" side of the permanent magnet rings, the iron pieces should only have a small influence on the calculated force and stiffness of the bearing. In order to test this assumption an axi-symmetric model of bearing II has been realized to analyse the influence of the iron pieces. In the axi-symmetric model we thus consider rings of permanent magnets and not the cubes considered in the full model. Using the axi-symmetric model we have calculated the axial force as well as the axial stiffness for a system both with and without iron pieces using the finite element software Comsol. The iron pieces were modelled with the full BH-curve of iron, as found in the Comsol Multiphysics model library. The result is that the relative change between the model without and with iron is smallest at the smallest distance between stator and the rotor. The relative change in the axial force without iron is -22% at $\delta z = 1$ mm and is -64% at $\delta z = 6$ mm. The relative change of the axial stiffness without iron is -15% at $\delta z = 1.5$ mm and -34% at $\delta z = 5.5$ mm. This will be discussed further in the comparison of the model data with the experimental results.

IV. Experimental

A. Characterization of the magnets

The magnets used for the bearings were commercial $3\times3\times3$ mm^3 NdFeB cubes, coated with Ni. The sizes were representatively ensured by measurement with a caliper. The coating is assumed to be around 20 μm, which gives the magnets a volume of about 0.026 cm^3.

The magnetic properties of the cube magnets were measured on a LakeShore 7407 Vibrating Sample Magnetometer (VSM). Four virgin magnets, taken directly from the box, were measured along with one removed from a bearing after force testing. No significant difference was observed between these five magnets and therefore only the results from one of the magnets is shown in Fig. 3.

Firstly, a magnet cube was mounted with the magnetization direction along the applied field direction. The magnetic field was then varied in the full range of the VSM from $\mu_0 H$ = 1.5 T to -1.5 T. Figure 3 shows the magnetization corrected for magnetostatic demagnetization. Here, a single value of N = 0.33 has been used, corresponding to the average value for a cube. The correction is done using the equation, $H = H_{\text{applied}} - NM$, where H is the magnitude of the internal field, H_{applied} is the magnitude of the applied field and M is the magnitude of the magnetization.

A remanence of 1.12 T is found for the measured magnet cube. A small drop in the magnetization can be seen when the internal field becomes negative in the second quadrant. The drop is about 3% and it is reversible. This is consistent with previous work [23], where it is ascribed to domains of less hard material that can be flipped when the field is reversed. It is assumed that it is caused by imperfections in the surface of the magnet cube. The available applied field of the VSM is not enough to reach the coercivity of the magnet cube, so the value of this must be more than 1.8 T. As the magnets in the models are modelled using a linear relation, and as they are operating in the second quadrant, their remanence is found by extrapolating the second quadrant magnetization to zero applied field, which results in a remanence of 1.09 T. The relative permeability is obtained by a linear fitting of the easy magnetization shown in Figure 3. In the first quadrant (0-1 T) the slope of the line is 1.0252(3), while in the linear part of the second quadrant (-0.5 to -1.5 T) it is 1.0394(2). Based on these values, we have adopted the value 1.04 for the easy axis relative permeability in our modeling.

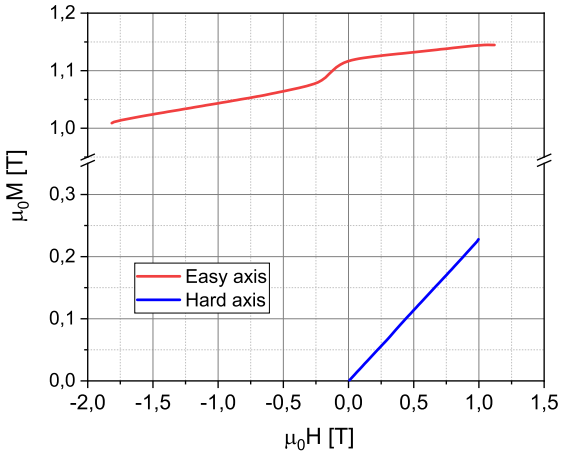

Fig. 3. Magnetization of a magnet cube in the easy and hard direction.

Rigidly mounting the cube with the field perpendicular to the field direction of the VSM allows probing of the off axis, or hard, permeability. The magnetization is found to be linear in the field, as expected; see Figure 3. The slope of the line gives an off-axis permeability of 1.247(2) and we therefore adopt a value of 1.25 for the relative permeability of the hard axes for modeling.

B. Force measurements

The stiffness and lift, and thus quality, of the magnetic bearings is analysed by measuring the force between the two parts of the bearing in different relative positions. One part of the bearing was rigidly mounted in the head of a workshop mill which could move with spatial accuracy in the $xy-$plane of $\pm$ 5 μm (controlled digitally) and 10 μm in the $z-$direction controlled manually via a dial gauge. Below this the second part of the bearing was held in a custom mounting connected with three perpendicular force transducers in order to measure the force between the two parts. 130 mm long and Ø5.0 mm Al rods connected the bearing mounting with HBM S2M force

transducers, thus ensuring a minimal transfer of torque upon application of an axial load. The lifting force transducer (z) was calibrated to measure up to 120 N while the two other components (x and y) where calibrated for measurements up to 10 N. The setup for measuring the force is shown in Fig. 4 and further details may be found in Ref. [13].

V. Results

A. Model results

Before testing the bearing experimentally, the optimal vertical placement of the single outer radially magnetized ring in Fig. 1, III was first investigated using the numerical model. In this geometry the position of the outer radial magnetized ring in the stator was varied. This distance is termed δd in Fig. 1.

Figure 5 shows the axial force and stiffness for Geometry III as function of the position of the radially magnetized ring. The axial clearance between the rotor and stator was kept fixed at 1 mm. As can be seen from the figure, there is a maximum in the axial force when $\delta d = 6$ mm. When the radially magnetized stator magnet is moved too high, so it passes the radially magnetized rotor ring the magnetic force from the stators radially magnetized ring starts pushing the rotor downwards, instead of providing lift. This means that the bearing loses axial stiffness. However, at a distance of $5 - 6$ mm the bearing has a significant lift while having the lowest radial stiffness. This is thus the optimal point of operation for this geometry.

B. Experimental results

The four bearings geometries illustrated in Fig. 1 were fabricated and experimentally tested in terms of their axial and radial forces as a function of axial and radial displacement of the rotor and stator parts, respectively. Geometry III was experimentally realized by choosing the optimal configuration as found through the modeling presented in the previous section. Thus the height δd is chosen to be 6 mm. As mentioned previously geometry IV has the same dimensions as geometry III, but has double rings, to investigate if this changes the stiffness of the bearing.

Figure 6 shows the axial force as a function of axial position (a) and radial position (b) with the corresponding model results also. For the radial position, the axial position is stated in the figure legend of (b). It is noted that the axial force transducer could not measure larger forces than 120 N while the radial transducers could measure up to about 15 N.

For geometry II the measured data did not agree with the model predictions. To obtain the agreement between the experimental results and the modeling data shown in Figure 6(a) and Figure 6(b) it has been assumed that the measured z-position of the rotor in bearing II was 0.4 mm too high. The same assumption has been made for geometry IV, but here only for the radial measurement. For this geometry the axial and radial measurements were done at different times and thus the possible systematic error of 0.4 mm in the axial position for the radial measurement is not necessarily present in both the axial and radial data sets. If the axial and radial data of bearing II and the radial data of bearing IV is not corrected, the experimental data has a much higher radial force compared to the model data. The systematic error of 0.4 mm could easily be introduced in the initial position of the bearing, as the distance between the top and bottom bearing was only measured relatively aside from a single initial calibration measurement. Thus the relative precision of the axial displacement is high, but there is a possible error in the absolute precision.

The good agreement between model and experiment confirms the relevance of the model presented above, and means that the model can be used to predict the performance of the bearing at different positions than those measured experimentally. The deviation between experimental and modeling results can be partly explained by the fact that the iron pieces have not been included in the model, as described previously and also by the possible systematic error in the axial position, as also discussed above.

To compare the radial performance of the different bearings, the model is used to calculate the radial force at the same axial displacement of 1 mm. Figure 7 shows the radial force at this axial displacement normalized by the lifting force provided by the bearing at zero radial displacement. From this figure, it is clear that geometry III has the lowest radial force per lifting force.

As can be seen from the figure, the normalized radial force increases linearly with radial displacement. The ratio between geometry I and III, i.e. without and with a single radially magnetized ring is constant at 0.383, i.e. geometry III has a much lower normalized radial force compared to geometry I. Interestingly for the double ring geometries, geometry II and IV, the additional of a radially magnetized ring results in a higher normalized radial force, which is not desirable in a bearing.

It should be noted that the fact that geometry III has the least negative radial stiffness relative to the lifting force of the tested geometries does not necessarily imply that it is the overall best geometry. The number of magnets, cost and weight could also be considered. However, given the relatively marginal cost of the permanent magnets, this consideration is likely to be of minor concern. It is further noted that the four bearings experimentally compared here are all of the same dimensions, i.e. they are directly comparable even though they have different amounts of magnets.

VI. Conclusion

A detailed magnetostatics model that calculates the force between two parts of a permanent magnetic bearing was presented. Based on the model an improved geometry for a passive magnetic bearing was suggested. It consists of one axially magnetized ring and one radially magnetized ring for both the stator and the rotor of the bearing. Four geometries were then realized experimentally with discrete cubic magnets of NdFeB. The experiments were designed such that the novel geometry could be compared to conventional geometries. In conclusion, the novel geometry has the overall best performance in terms of least radial stiffness per lifting force.

This article has been accepted for publication in a future issue of this journal, but has not been fully edited. Content may change prior to final publication. Citation information: DOI 10.1109/TMAG.2020.3042957, IEEE Transactions on Magnetics

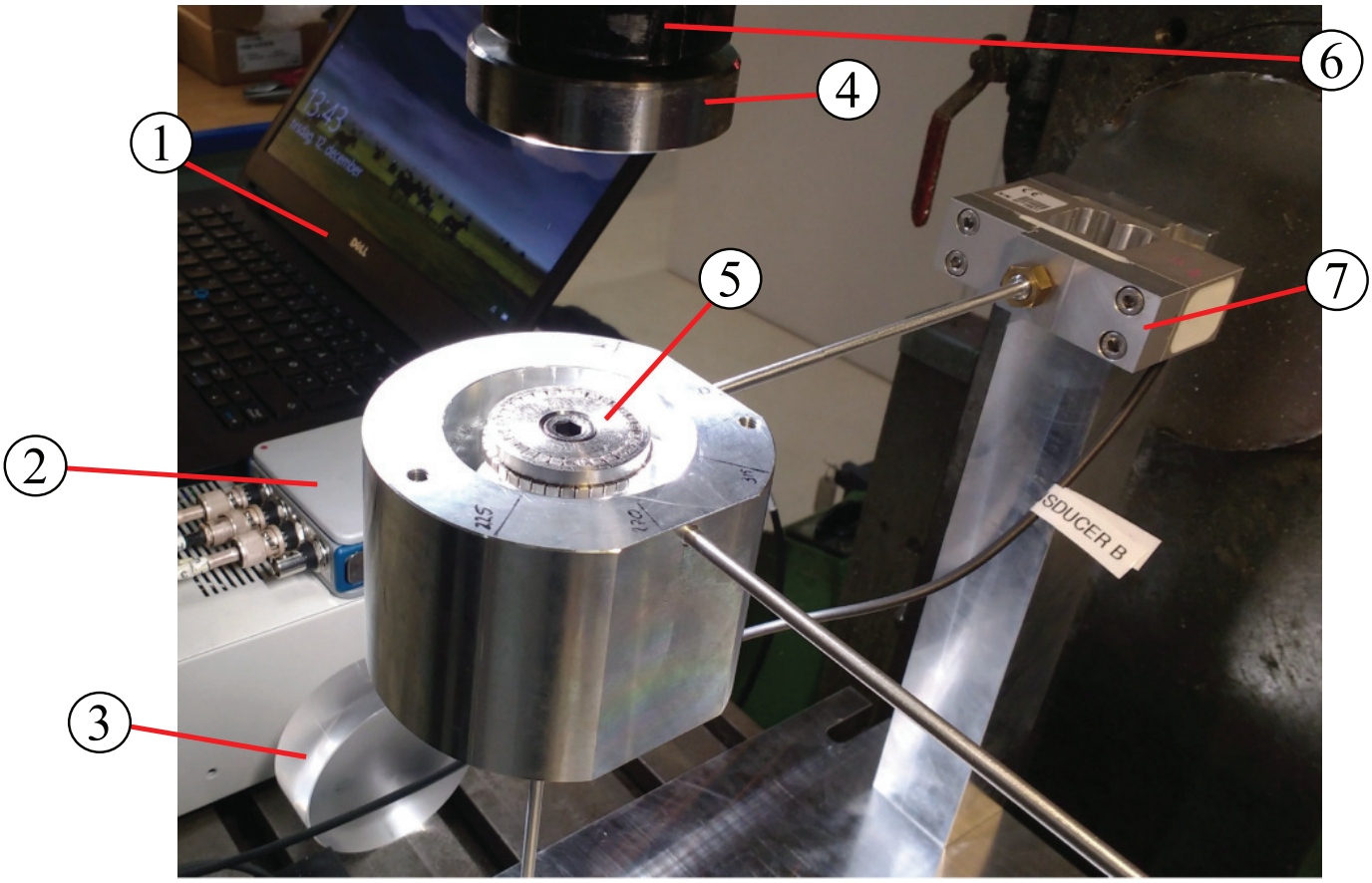

Fig. 4. The setup for measuring the force on the bearing. 1) Computer used with LabView to measure and process data, 2) Analog-to-digital converter, 3) Calibration cylinder (30 mm in height) for measuring the radial displacement, 4) Stator, 5) Rotor, 6) Shaft that can be moved vertically and horizontally in both directions, 7) Strain gauge used for measuring the radial and axial forces on the device. For further details see Ref. [13].

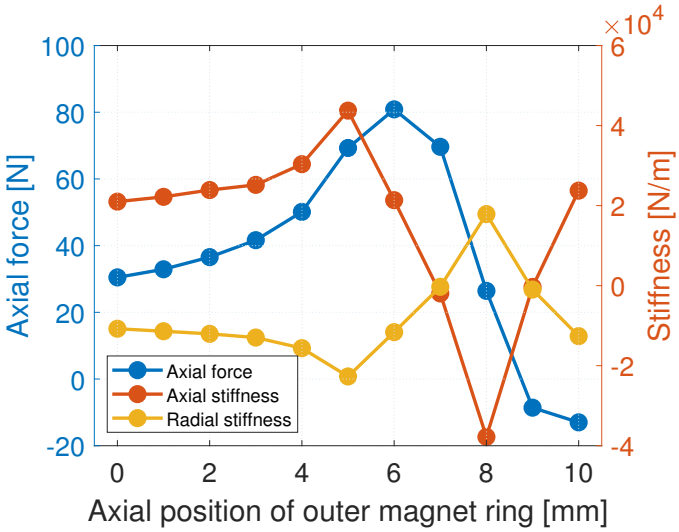

Fig. 5. The axial force and radial and axial stiffness of geometry III as function of the position of the radially magnetized ring in the stator. The side length of a magnet is 3 mm.

Acknowledgements

This work was financed by the Energy Technology Development and Demonstration Program (EUDP) under the Danish Energy Agency, project no. 64016-0058. The authors thanks the company WattsUp Power for many fruitful discussions and practical insights and also thank Paul Lagouanelle from Ecole Normale Superieure Paris-Saclay for assistance in measuring the axial and radial stiffness of the bearings.

References

[1] D. J. Griffiths. *Introduction to electrodynamics*. Pearson Education,, 2014.

[2] Michael Victor Berry. The levitrontm: an adiabatic trap for spins. *Proceedings of the Royal Society of London. Series A: Mathematical, Physical and Engineering Sciences*, 452(1948):1207–1220, 1996.

[3] Martin D Simon, Lee O Heflinger, and SL Ridgway. Spin stabilized magnetic levitation. *American Journal of Physics*, 65(4):286–292, 1997.

[4] J. P. Yonnet. Passive magnetic bearings with permanent magnets. *IEEE Transactions on Magnetics*, 14(5):803–805, 1978.

[5] J. P. Yonnet. Permanent magnet bearings and couplings. *IEEE Transactions on Magnetics*, 17(1):1169–1173, 1981.

[6] EP Furlani. A formula for the levitation force between magnetic disks. *IEEE Transactions on magnetics*, 29(6):4165–4169, 1993.

This article has been accepted for publication in a future issue of this journal, but has not been fully edited. Content may change prior to final publication. Citation information: DOI 10.1109/TMAG.2020.3042957, IEEE Transactions on Magnetics

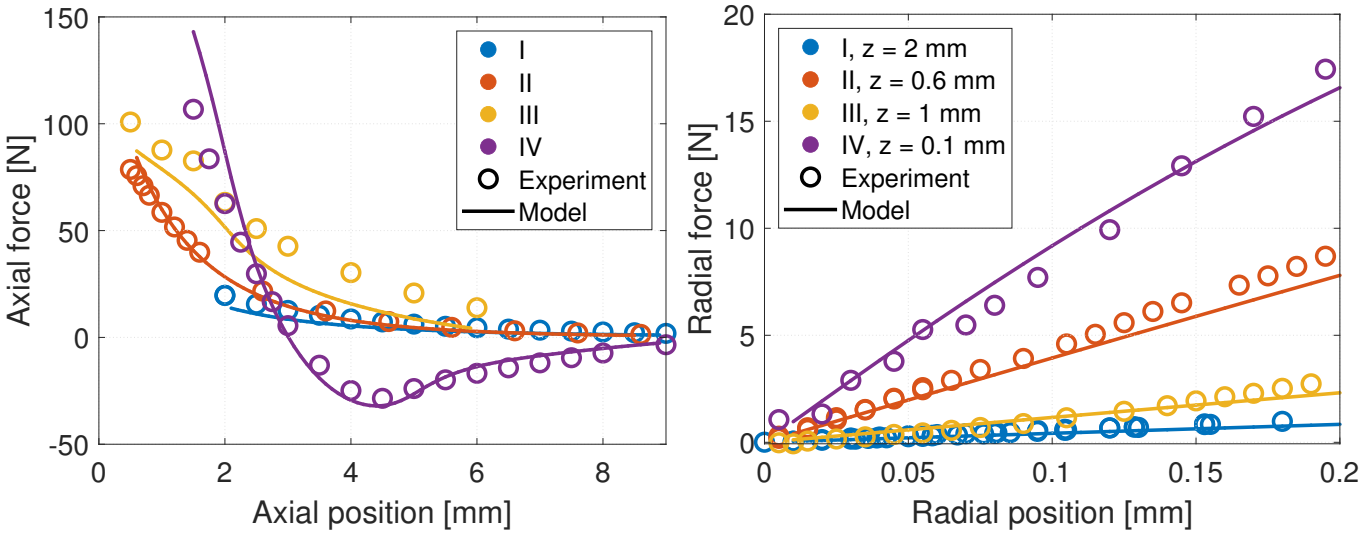

(a) Axial force as a function of axial position.

(b) Radial force as a function of radial position

Fig. 6. The axial force (a) as a function of axial position at the center position and the radial force (b) as a function of radial position at the axial position given in the legend.

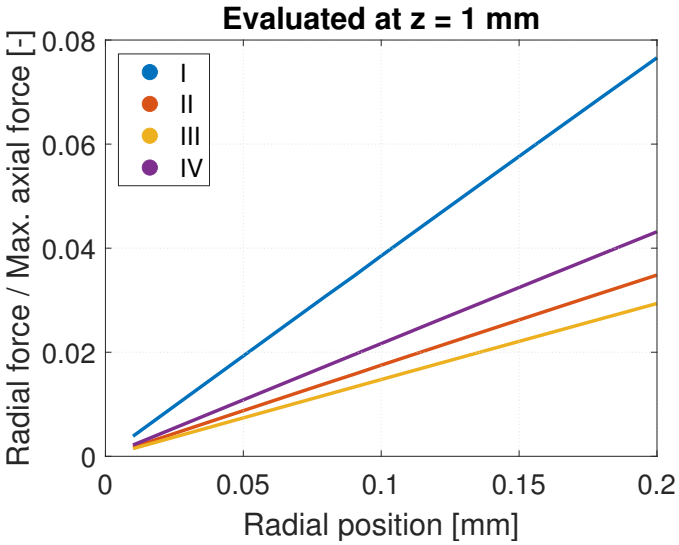

Fig. 7. The radial force at an axial separation of 1 mm normalized to the lifting force at this axial separation as computed using the model.

[7] R. Ravaud, G. Lemarquand, and V. Lemarquand. Force and stiffness of passive magnetic bearings using permanent magnets. part 1: Axial magnetization. *IEEE Transactions on Magnetics*, 45(9):3334–3342, 2009.

[8] R. Ravaud, G. Lemarquand, and V. Lemarquand. Force and stiffness of passive magnetic bearings using permanent magnets. part 2: Radial magnetization. *IEEE Transactions on Magnetics*, 45(7):2996–3002, 2009.

[9] R. Ravaud, G. Lemarquand, and V. Lemarquand. Halbach structures for permanent magnets bearings. *Progress in Electromagnetics Research M*, 14:263–277, 2010.

[10] Brad Paden, Nelson Groom, and James F Antaki. Design formulas for permanent-magnet bearings. *Journal of Mechanical Design*, 125(4):734–738, 2003.

[11] A. Vuckovic, N. Raicevic, S. Ilic, S. Aleksic, and M. Peric. Axial force calculation of passive magnetic bearing. *Serbian Journal of Electrical Engineering*, 11(4):649–660, 2014.

[12] Pranab Samanta and Harish Hirani. Magnetic bearing configurations: Theoretical and experimental studies. *IEEE Transactions on Magnetics*, 44(2):292–300, 2008.

[13] Nikolaj Aleksander Dagnæs-Hansen and Ilmar F. Santos. Permanent magnet thrust bearings for flywheel energy storage systems: Analytical, numerical, and experimental comparisons. *Proceedings of the Institution of Mechanical Engineers, Part C: Journal of Mechanical Engineering Science*, 233(15):5280–5293, 2019.

[14] Roland Moser, Jan Sandtner, and Hannes Bleuler. Optimization of repulsive passive magnetic bearings. *IEEE transactions on magnetics*, 42(8):2038–2042, 2006.

[15] Jean-Paul Yonnet, Guy Lemarquand, Sophie Hemmerlin, and Elisabeth Olivier-Rulliere. Stacked structures of passive magnetic bearings. *Journal of Applied Physics*, 70(10):6633–6635, 1991.

[16] K. Bachovchin, J. Hoburg, and R. Post. Magnetic field and forces in permanent magnet levitated bearings. *IEEE Transactions on Magnetics*, 48(7):2112–2120, 2012.

[17] Alexei V Filatov, Eric H Maslen, and George T Gillies. A method of noncontact suspension of rotating bodies using electromagnetic forces. *Journal of Applied Physics*, 91(4):2355–2371, 2002.

[18] Will Robertson, Ben Cazzolato, and Anthony Zander. Axial force between a thick coil and a cylindrical permanent magnet: Optimizing the geometry of an electromagnetic actuator. *IEEE Transactions on magnetics*, 48(9):2479–2487, 2012.

[19] Zhenzhong Su, Dong Wang, Junquan Chen, Xianbiao Zhang, and Leitao Wu. Improving operational performance of magnetically suspended flywheel with pm-biased magnetic bearings using adaptive resonant controller and nonlinear compensation method. *IEEE Trans-*

actions on Magnetics, 52(7):1–4, 2016.

[20] Mousa Lahdo, Tom Ströhla, and Sergej Kovalev. Repulsive magnetic levitation force calculation for a high precision 6-dof magnetic levitation positioning system. *IEEE Transactions on Magnetics*, 53(3):1–6, 2016.

[21] R. Bjørk and K. K. Nielsen. MagTense. Technical University of Denmark, DTU Energy, Department of Energy Conversion and Storage. https://doi.org/10.11581/DTU:00000071 . http://www.magtense.org, 2019.

[22] A. Smith, K. K. Nielsen, D. Christensen, C. R. H. Bahl, R. Bjørk, and J. H. Hattel. The demagnetizing field of a non-uniform rectangular prism. *Journal of Applied Physics*, 107(10):103910, 2010.

[23] I. Petrov, D. Egorov, J. Link, R. Stern, S. Ruoho, and J. Pyrhonen. Hysteresis losses in different types of permanent magnets used in pmsms. *Ieee Transactions on Industrial Electronics*, 64(3):7444147, 2502–2510, 2017.